JOURNAL OF THERMOPHYSICS AND HEAT TRANSFER
Vol. 8, No. 4, Oct.–Dec. 1994

Heat Transfer in Two-Phase Flow Through a Circular Tube at Reduced Gravity

Raymond W. Rite* and Kamiel S. Rezkallah†
University of Saskatchewan, Saskatoon, Saskatchewan S7N 0W0, Canada

A two-phase, two-component flow test loop was flown onboard NASA's KC-135 Zero-*g* aircraft in October 1992. During the flights, flow regime, pressure gradient, and heat transfer data were simultaneously gathered for an air-water mixture in vertical, cocurrent, upward flow through a circular tube with a diameter of 9.53 mm. The range of flow rates studied consisted of superficial liquid velocities from 0.24 to 3.0 m/s, and superficial gas velocities between 0.2–17 m/s. Heat transfer measurements taken during μ-*g* were compared with heat transfer data gathered at 1 *g* with the same test loop. This comparison indicated that at low liquid and gas velocities heat transfer coefficients at 1 *g* were up to 15% greater than those measured in μ-*g*. At higher liquid or gas velocities this trend was reversed, and microgravity flows yielded heat transfer coefficients approximately 10% higher than the corresponding 1 *g* flows. It was found that a change in the flow regime was not responsible for this difference in heat transfer coefficients.

Nomenclature

B = bias limit
c_p = specific heat at constant pressure
D = inner tube diameter
dx = differential length
g = gravitational acceleration
h = convective heat transfer coefficient
L_h = length of heated test section
P = precision limit
Pr = Prandtl number
Q = heat
Re = Reynolds number
T = temperature
t = time
U = total uncertainty
V = velocity
V^* = normalized velocity
w = mass flow rate
x = mass quality, $w_G/(w_L + w_G)$
γ = coefficient of correlation
δ = Kronecker delta
η = normalized heat transfer coefficient
Θ = normalized temperature difference
μ = dynamic viscosity
ρ = density
σ = standard deviation

Subscripts

d = dwell, fluid residence
f = fluid
G = single-phase gas
i = index for differential section of heater
j, k, l = indices in bias limit equation
L = single-phase liquid
SG = superficial gas
SL = superficial liquid
s = inner tube surface
TP = two-phase, two-component

Presented as Paper 93-2851 at the AIAA 28th Thermophysics Conference, Orlando, FL, July 6–9, 1993; received Oct. 18, 1993; revision received May 9, 1994; accepted for publication May 11, 1994.

*Graduate Student, Mechanical Engineering Department. Student Member AIAA.

†Professor, Mechanical Engineering Department, Director, Microgravity Research Group. Member AIAA.

Introduction

SEVERAL studies have been done on pool boiling in microgravity situations. Among these are studies by Merte and Clark[1] and Siegel.[2] However, there is little data on heat transfer in a forced-convective situation with two-phase, single-component flows under microgravity conditions, and absolutely no data on two-component flows.

For single-component flows, Papell[3] performed a study on instability effects in two-phase, subcooled water flows. Using a test aircraft to obtain microgravity conditions, Papell found a 16% increase in the heat transfer coefficient during microgravity durations as opposed to 1 *g* conditions. Papell hypothesized that the increase was due to a transition from bubbly flow to slug flow as a result of the reduction in gravity. This could not be verified since no flow observations were made during the experiment. Extrapolation of existing mathematical models for 1 *g* flows by Reddy et al.[4] showed that bubbly flow may not exist under microgravity conditions, but more recent experimental data by Zhao and Rezkallah[5] and Dukler et al.[6] indicate that bubbly flow is present under microgravity conditions. Therefore, the validity of Papell's hypothesis is questionable.

Feldmanis[7] examined the pressure and temperature response of a boiling and condensing water flow to the changes in gravitational acceleration onboard NASA's KC-135 aircraft. Four fluid temperatures were recorded at four locations around the flow loop: 1) the cooling water inlet and 2) outlet temperatures, 3) condensing temperature, and 4) evaporating temperature. An increase in the condensate temperature was recorded as gravity was reduced. It was conjectured that this increase was due to either a reduced condensation heat transfer coefficient or increased evaporation rates. Feldmanis postulated that under forced-convective condensation conditions gravity effects could be neglected, so that higher evaporation rates were indeed the probable cause of the condensate temperature increase. However, neither boiling nor condensing heat transfer coefficients were determined by Feldmanis.

In a recent study of forced convective two-phase, single-component flow, Hill and Best[8] worked with a boiling and condensing dichlorodifluoromethane (Refrigerant 12) test loop onboard the KC-135. This test loop consisted of a two-part tube-in-tube condenser. The first part was a transparent condenser that permitted flow observation, the second part was

made of copper and was instrumented to allow for measurements of heat transfer coefficients. The evaporator section also consisted of an aluminum tube wrapped with an electrical resistance heater. Both the condenser and evaporator were oriented horizontally with respect to the floor of the plane. It was reported that the condensation heat transfer coefficients were 26% lower for μ-g conditions as opposed to 1 g conditions. Boiler temperatures remained constant throughout the KC-135 flights. Thus, no conclusions could be drawn on the effect of acceleration on the boiling heat transfer coefficients.

Experimental Facility

A two-phase, two-component test apparatus was designed and built at the University of Saskatchewan for the performance of microgravity experiments on NASA's KC-135 Zero-g aircraft. The apparatus is instrumented such that simultaneous measurements of pressure drop and heat transfer data can be made, as well as continuous observation and recording of the two-phase flow patterns. In order to cover a wide range of test conditions, the facility allows for the independent control of three separate parameters during testing: 1) airflow rate, 2) water flow rate, and 3) temperatures of the two-phase mixture in the flow loop.

The test loop can be divided into two main sections: 1) the hardware components required to obtain the conditions desired during a certain run, and 2) the data acquisition system to record the various parameters. A schematic of the test apparatus is shown in Fig. 1. Onboard the plane the apparatus was situated horizontally with the floor of the aircraft. A complete discussion of the flow loop may be found by Rite and Rezkallah.[9] In addition, more details concerning the heated test section (which is of primary importance in this work) will be provided here.

After air is combined with water in the mixer (shown in the lower left corner of the schematic in Fig. 1), the two-phase mixture then proceeds through a 74-cm-long flow developing section made of stainless steel with an i.d. of 9.53 mm ($L/D \approx 77$). A 16.2-cm-long ($L/D \approx 17$) observation section follows as shown in Fig. 1. The observation section is constructed of 9.53-mm-i.d. acrylic tubing. Thus, from the exit of the mixer to the heated test section, the total calming length is 94 tube diam. This provides for a fully developed velocity profile for heat transfer coefficient measurements in the heated test section.

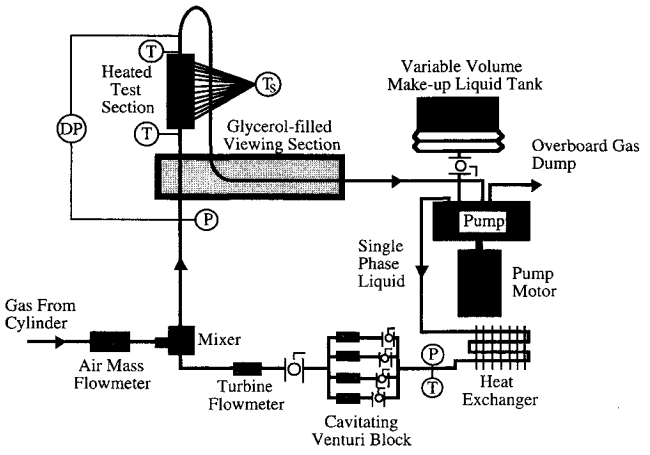

Fig. 1 Schematic of the two-phase, microgravity test facility.

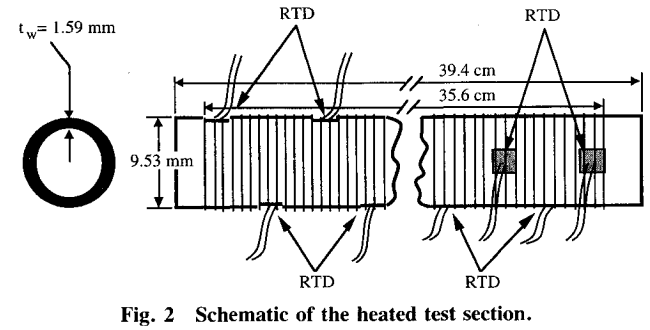

Fig. 2 Schematic of the heated test section.

Following the observation section, the temperature of the mixture is measured with a 3.18-mm-diam, 10-cm-long resistance temperature device (RTD) that is inserted transversely into the flow. In order to minimize any interference with the flow, which could cause a distortion of the flow pattern and lead to changes in pressure drop as well as heat transfer coefficients, a special fixture was designed for the RTD. The fixture consists of an acrylic Tee section with a 9.53 mm i.d. for the straight-through section, and a 6.35 mm i.d. branch. In the branch, an RTD is inserted such that its tip is flush with the inner wall of the straight-through section. This allows the entire length of the probe to be immersed in the two-phase mixture, but at the same time minimizes the disturbance to the flow.

The inlet temperature RTD fixture is followed by the heated test section shown schematically in Fig. 2. It consists of a 9.53-mm-i.d. copper tube having a wall thickness of 1.59 mm. The copper tube has a total length of 39.4 cm, of which 35.6 cm are heated. Twelve platinum RTDs (10 were operational during the flights and during ground data acquisition) are spaced evenly along the 35.6-cm heated section and are held in place with the heater wire. A thermal conductive ZnO_2 paste with a nominal, specific thermal resistance of 0.058°C-cm^2/W was placed between the RTDs and the tube to achieve good thermal contact.

The heater wire is a 28 AWG varnished copper wire. The wrapping was done in two separate sections wired in parallel to allow for the necessary power requirements without exceeding the amount of available amperage. This permits up to 1000 W of total heat addition to the two-phase mixture for a maximum power flux of 94 kW/m^2. In order to minimize heat losses to the ambient from the heater during operation, 50 mm of a high-temperature, ceramic fiber insulation was packed around the heater. In addition, a 20-mm-thick blanket of fiberglass insulation was wrapped around the entire structure. The latter was covered with an aluminum sheet metal casing.

At the outlet of the heated test section, another 3.18-mm RTD is used to measure outlet temperature. This temperature probe is inserted axially into the outlet flow, allowing for complete immersion in the gas-liquid mixture. Interference with the flow pattern was not a consideration here.

All data acquisition functions were handled by a 286 PC equipped with 12-bit analog-to-digital conversion using a successive approximation algorithm. A BASIC computer program was used to acquire the data once every 0.8 s and to control the airflow rate.

Experimental Procedure

NASA's KC-135 Zero-g aircraft was utilized to obtain the required microgravity test conditions. The flight path of the aircraft is a Keplerian one, as shown in Fig. 3. Approximately 23 s of near zero gravity (or microgravity) is produced while the aircraft is at the crests of the flight path. Between the crests, the vertical gravitational acceleration of the plane transitions from microgravity to approximately 1.8 g. The approximate time durations of the microgravity portions of the flight and the transition periods between them are shown in Fig. 3. It should be noted, however, that not all 23 s of the microgravity time period may be utilized. A maximum criterion for gravity divided by normal Earth gravity (g/g_0) of 0.04 was imposed. This resulted in a useful window of only 10–16 s for most parabolas. In addition, some parabolas that failed to meet this g-level criterion were rejected outright.

Six flights were flown over two weeks in October 1992. Each flight consisted of four sets of 10 parabolas. There was

Table 1 Flight test matrix for the afternoon flight of October 15, 1992

Parabola number	V_{SL}, m/s	V_{SG}, m/s	Q, W	Parabola number	V_{SL}, m/s	V_{SG}, m/s	Q, W
1	0.9	0.2	500	21	2.5	0.2	650
2	0.9	0.3	500	22	2.5	0.3	650
3	0.9	0.5	500	23	2.5	0.45	650
4	0.9	0.9	500	24	2.5	0.9	650
5	0.9	1.5	500	25	2.5	1.5	650
6	0.9	3.0	500	26	2.5	3.0	650
7	0.9	5.0	500	27	2.5	5.0	650
8	0.9	8.0	500	28	2.5	8.0	650
9	0.9	12.0	500	29	2.5	12.0	650
10	0.9	20.0	500	30	2.5	20.0	650
11	2.0	0.2	600	31	3.0	0.2	700
12	2.0	0.3	600	32	3.0	0.3	700
13	2.0	0.45	600	33	3.0	0.45	700
14	2.0	0.9	600	34	3.0	0.9	700
15	2.0	1.5	600	35	3.0	1.5	700
16	2.0	3.0	600	36	3.0	3.0	700
17	2.0	5.0	600	37	3.0	5.0	700
18	2.0	8.0	600	38	3.0	8.0	700
19	2.0	12.0	600	39	3.0	12.0	700
20	2.0	20.0	600	40	3.0	20.0	700

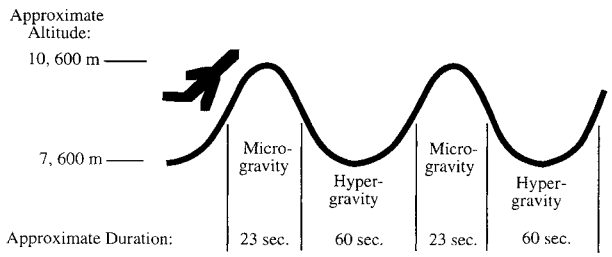

Fig. 3 KC-135 Keplerian flight trajectory.

approximately a five-min break between each set of 10. For each flight, a test matrix was designed to specify liquid and gas velocities and the heated test section power. The gravitational acceleration in the z-axis (up-down relative to the plane floor) was then used by the computer to keep track of the parabola number so that the desired test conditions for that parabola could be obtained. A typical flight consisted of maintaining a constant liquid velocity for 10 parabolas, while increasing the gas velocity for each parabola. The liquid velocity would then be changed for the next 10 parabolas, and the gas velocity would then be increased in a stepwise fashion. This method was pursued in order to obtain as wide a coverage of the flow pattern map as possible. A test matrix for one of the October flights is shown in Table 1.

Experimental Data Reduction

Transient Effects

Due to the short duration of microgravity onboard the KC-135, it is important to consider whether "quasisteady" heat transfer coefficients for two-phase, convective flow can be measured. Does the system respond quickly enough to allow for such measurements? There are two sources of transients during any flight test: one is due to the variation of the gravity field; and the other is due to changing the air and water flow rates and the heater power. The effects of both of these transients were investigated experimentally, and the results are reported here.

The effects of the gravity and set point transients were first addressed by Rite and Rezkallah.[9] In this work it was shown that in annular, slug-annular transition and slug flow regimes, the change of gravity had an effect on the heat transfer coefficients. However, in bubbly and bubbly-slug transition flows no change in the heat transfer coefficients was evident as the gravity level varied. The change in the heat transfer coefficients was mainly associated with a change in flow regime due to changes in gravity. It was also shown that the set point transient time was approximately 20 s at the highest liquid flow rates, and approximately 10 s at the lower liquid flow rates. Even with the highest liquid flows, it was found that the temperature difference between the inner tube surface and the bulk fluid temperature was within 10% of the steady-state value after about 10 s. For these tests, a sudden change in the heat input was used to induce a transient on the system.

In order to determine how quickly a change in the flow regime could affect the measured heat transfer coefficients, an additional experimental transient investigation was undertaken on-ground in which the gas flow was increased instantaneously in order to precipitate a flow regime transition. The results at V_{SL} = 1.2, 0.5, and 0.1 m/s are shown in Figs. 4a, 4b, and 4c, respectively. In the figure, the difference between the average surface and fluid temperatures, as well as the superficial gas and liquid velocities, are plotted for 60 s after an increase in the gas velocity at time t = 0 from 0.2 to 10 m/s. All three quantities have been normalized as follows:

$$\Theta = \frac{(T_{s,\text{avg}} - T_{f,\text{avg}}) - (T_{s,\text{avg}} - T_{f,\text{avg}})_{\text{initial}}}{(T_{s,\text{avg}} - T_{f,\text{avg}})_{\text{final}} - (T_{s,\text{avg}} - T_{f,\text{avg}})_{\text{initial}}} \quad (1)$$

$$V^*_{SL} = \frac{V_{SL}}{V_{SL,\text{avg}}} \quad (2)$$

$$V^*_{SG} = \frac{V_{SG} - V_{SG,\text{initial}}}{V_{SG,\text{final}} - V_{SG,\text{initial}}} \quad (3)$$

In each of the cases in Fig. 4, a gas velocity change induces a change in the flow pattern as follows: slug-to-annular for V_{SL} = 1.2 m/s, bubbly-slug transition to churn-annular transition for V_{SL} = 0.5 m/s, and slug-churn to annular for V_{SL} = 0.1 m/s. It can be seen that as the liquid velocity increases, the time required for steady-state temperatures to be achieved increases just as was found in Rite and Rezkallah.[9] This is expected since the heat capacity of the two-phase mixture $(wc_p)_G + (wc_p)_L$, increases as the liquid flow rate increases. Thus, the thermal response of the heated test section will be slower as the heat capacity of the two-phase mixture is increased. However, it can also be seen that even in the worst case (V_{SL} = 1.2 m/s), the temperature difference between the surface and the fluid essentially reaches its steady-state value after the first 10 s. The dwell times t_d for both the liquid and the gas flows are presented in Table 2. In the table it can be seen that the dwell times for both the liquid and the gas are less than the transient time that was observed. Therefore, the

Table 2 Dwell times for the liquid and gas flows

V_{SL}, m/s	V_{SG}, m/s	$t_{d,L}$, s	$t_{d,G}$, s
0.10	10.0	3.56	0.036
0.50	10.0	0.71	0.036
1.20	10.0	0.30	0.036

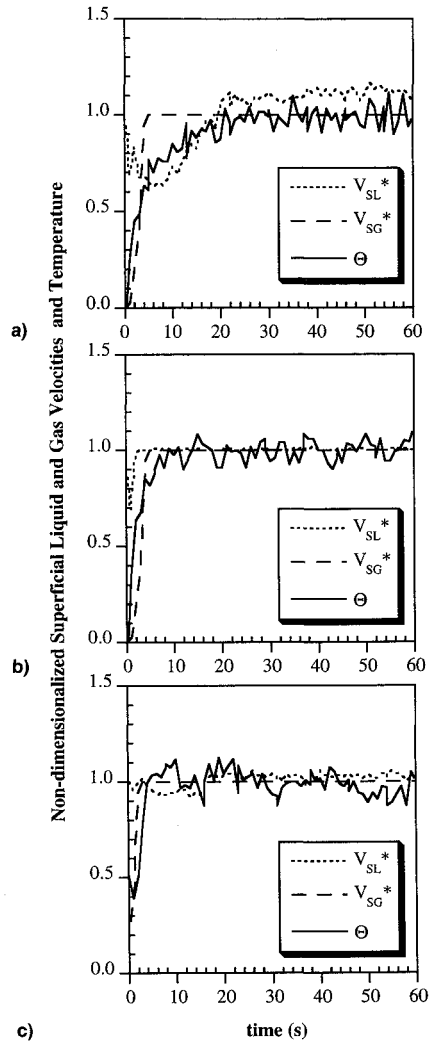

Fig. 4 Thermal response of the heated test section with flow regime transition.

liquid inventory inside the tube should be rearranged in accordance to the new equilibrium void fraction.

Based on the findings above, it was decided to use only the data collected during the last 8–10 s of the microgravity portions of each parabola in order to minimize the impact of the thermal transient on the reported heat transfer measurements. This approach was adopted for all data points for the sake of uniformity even though the actual transient response varies with the liquid flow rate and the flow regime. This was also reported by Rite and Rezkallah.[9]

Calculation of Experimental Heat Transfer Coefficients

The experimentally determined average heat transfer coefficients, both single- and two-phase, were arrived at by first evaluating the local heat transfer coefficients at 10 discrete sections of the heated test section, where the tube wall temperatures were measured. These local convective heat transfer coefficients were evaluated using the equation

$$h_i = [Q/\pi L_h D(T_{s,i} - T_{f,i})] \tag{4}$$

For this equation, the heat flux was assumed to be uniform for the entire length of the heated test section and constant. The measured electrical power to the heater and the heated test section surface area were used to calculate the heat flux. It was determined from ground tests that the test section outer insulation provided enough thermal resistance such that there was insignificant heat loss to the ambient. The inner tube wall surface temperature was calculated from the measured outer surface temperature by assuming one-dimensional conduction through a cylindrical tube wall. The air-water mixture temperature could only be measured at the inlet and outlet of the heated test section, so local bulk fluid temperatures were interpolated from the inlet and outlet fluid temperatures using a linear temperature profile. The inlet and outlet fluid temperatures were measured with RTD probes as mentioned previously.

After the determination of the local heat transfer coefficients with Eq. (4), an average heat transfer coefficient was calculated based on the integration of the local values with the equation

$$h = \frac{1}{L_h}\int_0^{L_h} h_i \, dx \tag{5}$$

In this integration, it was decided to discard the two local heat transfer coefficients near the inlet and the outlet of the heated test section because of axial conduction effects. Therefore, the reported average two-phase heat transfer coefficients are based on the remaining eight local heat transfer measurements.

Error Analysis

The heat transfer coefficients to be reported for both flight and ground data are presented in terms of the normalized two-phase heat transfer coefficient η. The total uncertainty U_η in this nondimensional heat transfer coefficient includes a precision uncertainty P_η, and a bias uncertainty B_η. Following the method of Coleman and Steele,[10] the rss total uncertainty can be expressed in the form:

$$U_\eta = (B_\eta^2 + P_\eta^2)^{1/2} \tag{6}$$

For the above equation, the precision uncertainty (or precision limit) was calculated to range from 0.068 at the highest liquid velocities reported to 0.70 at the lowest velocities. This was based on the average standard deviation of the data that was measured both onboard the KC-135 for several flights, and on-ground in the laboratory for a number of repeated trials at the same set point with a confidence level of 95% (i.e., for a Gaussian distribution, 95% of the readings will be within $\pm 1.96\sigma$ of the mean).

By normalizing the heat transfer data, the bias limit in Eq. (6) is substantially reduced. It was shown by Chakroun et al.[11] that the experimental error may be reduced significantly when the experimental data are normalized with respect to a baseline condition. In the present case, the baseline condition is the single-phase heat-transfer coefficient at the corresponding liquid Reynolds number Re_{SL}.

In Eq. (4), h_i was shown to be a function of Q, L_h, D, $T_{s,i}$, and $T_{f,i}$. Thus, the average two-phase heat transfer coefficient h_{TP} will also be a function of these parameters. The single-phase heat-transfer coefficients were also calculated with the same variables listed in Eq. (4). It should be noted, however, that single-phase data was not taken at each two-phase data point. Instead, correlations were used to determine h_L as a function of Re_{SL} and Pr_L.

Since Re_{SL} and Pr_L are calculated using the parameters: V_{SL}, ρ_L, D, C_p, k_L, and μ_L, the single-phase heat transfer coefficient will be a function of these parameters, in addition to those from Eq. (4). It can be seen that Q, L_h, $T_{s,i}$, and $T_{f,i}$ are perfectly correlated between the single- and two-phase

data. Therefore, any bias error in their measurements will be eliminated. This can be further verified by evaluating the bias limit equation:

$$B_\eta = \sum_{k=1}^{J} \left[\left(\frac{\partial \eta}{\partial x_k} \right)^2 B_k^2 + \sum_{l=1}^{J} \left(\frac{\partial \eta}{\partial x_k} \frac{\partial \eta}{\partial x_l} \right) \gamma_{kl} B_k B_l (1 - \delta_{kl}) \right]^{1/2} \tag{7}$$

where X_l and X_k are any of the measured variables: Q, L_h, $T_{s,i}$, $T_{f,i}$, V_{SL}, ρ_L, D, C_p, k_L, and μ_L; B_l and B_k are the bias limits of these variables; and γ is 1.0 for the perfectly correlated variables (Q, L_h, $T_{s,i}$, and $T_{f,i}$), and 0 for the uncorrelated variables (V_{SL}, ρ_L, D, C_p, k_L and μ_L). In Eq. (7), it can be shown that the partial derivatives of η with respect to Q, L_h, $T_{s,i}$, and $T_{f,i}$, for single- and two-phase data will cancel each other. This leaves V_{SL}, ρ_L, D, C_p, k_L, and μ_L as uncorrelated variables. With a bias uncertainty in the curve fit properties ρ_L, C_p, k_L, and μ_L, of 1.0%, bias uncertainties in the measurements of the dimension D of 1.0%, and in V_{SL} of 1.0% for $V_{SL} < 0.80$ m/s, and 1.8% for $V_{SL} > 0.80$ m/s, the total uncertainty in η can then be calculated with Eq. (6). The total uncertainty was found to range from approximately 0.071 to 0.70, with decreasing liquid velocity (increasing η) or 14.2%, nominally.

In addition to the uncertainty in η, there is also an uncertainty associated with the mass quality x, which is used in plotting the data. Using the same analysis method described above for η, the total uncertainty in x was estimated to have a nominal value of 0.00032 or 7.6%.

Experimental Results

In order to assess the impact of microgravity on two-phase, two-component convective heat transfer coefficients, the two-phase heat transfer data collected onboard the KC-135 were also collected on-ground using the same test apparatus. A comparison of the two sets of data is shown in Figs. 5–8. In the figures, the nondimensionalized two-phase heat transfer coefficients are shown plotted as a function of the gas quality. In all tests, V_{SL} was held constant at eight different set points while the gas velocity was increased. The flow regime for each data point collected is also shown next to each data point in the figures. A comparison of these flow regime results with some of the currently available flow maps may be found in Ref. 5. The abbreviations for the microgravity flow regimes are as follows: B: bubbly flow, B-S: bubbly-slug transitional flow, S: slug flow, S-A: slug-annular transitional flow, and A: annular flow. In addition, with the ground data, churn flow and transitions to churn flow were also observed. These

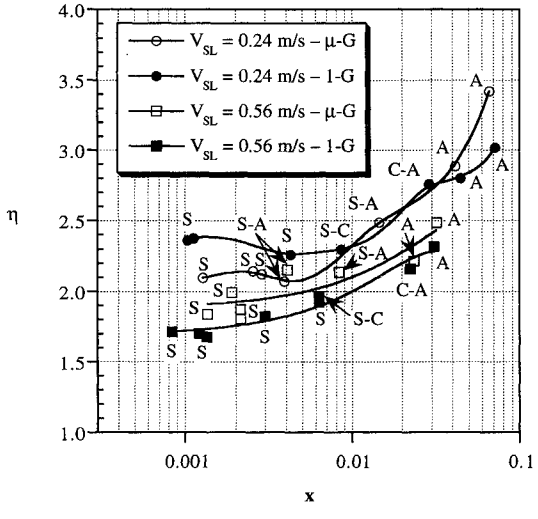

Fig. 5 Normalized two-phase heat transfer coefficient vs quality for V_{SL} = 0.24 and 0.56 m/s.

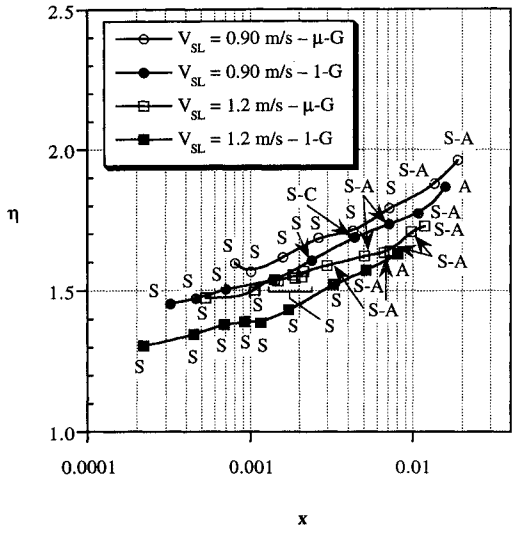

Fig. 6 Normalized two-phase heat transfer coefficient vs quality for V_{SL} = 0.90 and 1.2 m/s.

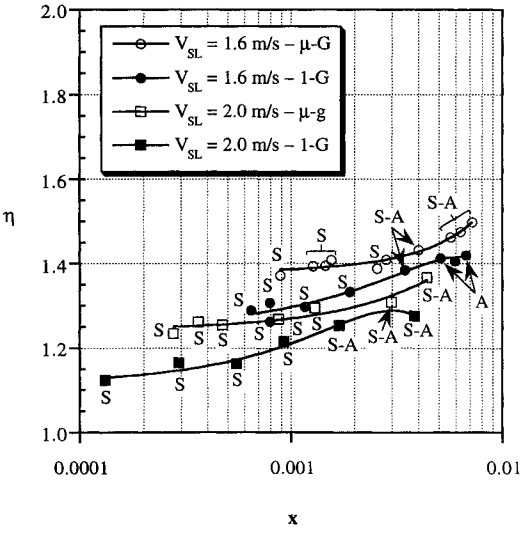

Fig. 7 Normalized two-phase heat transfer coefficient vs quality for V_{SL} = 1.6 and 2.0 m/s.

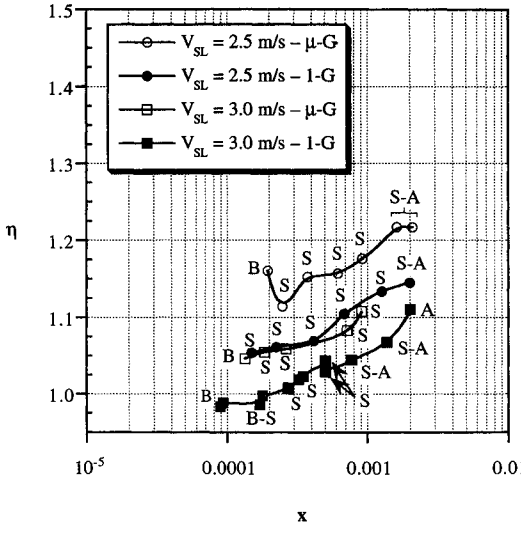

Fig. 8 Normalized two-phase heat transfer coefficient vs quality for V_{SL} = 2.5 and 3.0 m/s.

are abbreviated as follows: S-C: slug-churn transitional flow, C: churn flow, and C-A: churn-annular transitional flow.

Figure 5 shows the data for the two lowest liquid velocities: V_{SL} = 0.24 and 0.56 m/s. The liquid superficial velocities for all the data points shown in the graph were maintained within a coefficient of variation of 4.3% of the average value. In this figure it can be seen that for V_{SL} = 0.24 m/s the normalized heat transfer coefficients at 1 *g* are approximately 15% higher than the μ-*g* data at the lowest qualities. As the quality is increased, the difference between the two sets decreases until at approximately x = 0.008 there is a crossover in the normalized heat transfer coefficient. From this point, the 1 *g* coefficients are slightly larger than their microgravity counterparts. It can also be seen that the flow regimes for both ground and flight data are in the slug flow regime up until x = 0.01. At this point the regimes transition to slug-annular for the μ-*g* data and slug-churn for the 1 *g* data. For V_{SL} = 0.56 m/s, the microgravity data is higher than the 1 *g* data, but only by 5–10%, with points at x = 0.002 and 0.02 being essentially the same for 1 *g* and μ-*G*.

Figure 6 shows the normalized two-phase heat transfer coefficients for V_{SL} = 0.9 m/s and 1.2 m/s. For these points, the liquid velocity was maintained for both flight and ground data within 3.2% of the mean value. The difference between the microgravity and the Earth gravity heat transfer coefficients for both liquid velocities is on the order of 7%, with the μ-*g* data being consistently higher than the 1 *g* data for all qualities. It can be seen that as the quality is increased, the difference between μ-*g* and 1 *g* flows decreases. This is consistent with the fact that the shear forces should become dominant as the gas velocity is increased, hence, the influence of gravity is minimized. Also, it should be noted that there is not a marked change in η as the flow regime changes.

The results for the higher liquid flow rates (V_{SL} = 1.6, 2.0 m/s) are shown in Fig. 7. In these cases, V_{SL} was maintained within 3.6% of the mean value. For both cases, the microgravity normalized heat transfer coefficients are higher than the 1 *g* heat transfer coefficients. With V_{SL} = 1.6 m/s, the difference is at most 7% for x up to 0.007. For V_{SL} = 2.0 m/s, the difference is of approximately the same order.

Figure 8 shows the normalized heat transfer coefficients for the highest liquid velocities; V_{SL} = 2.5 and 3.0 m/s. For these two liquid set points the liquid velocity was maintained within 2.9% of the desired value for both ground and flight data. In this figure, it can be seen that the microgravity data are consistently 7–10% higher than the corresponding ground data. Again, this difference is not accompanied by a major change in the flow regime for either data set.

An examination of the pressure drop results for the same flight and ground data in the transitional slug and annular flow regimes reveals that at high liquid and gas velocities, the difference between 1 *g* and μ-*g* pressure drop was negligible. However, at low flow rates the pressure drop at microgravity was found to be higher than at normal Earth gravity.[12] It has been shown by Vijay et al.[13] and others that trends in heat transfer coefficients follow trends in pressure drop. The pressure drop trends found in the study by Zhao and Rezkallah[12] do seem to be similar to what was found in terms of heat transfer for data points in the slug-annular and annular flow regimes. In these regimes, the μ-*g* heat transfer coefficients were higher than 1 *g* with the difference diminishing as the gas velocity increased.

One possible explanation for the difference in the heat transfer coefficients in slug flow involves the length of the liquid slugs as discussed by Collier[14] in the context of circulation effects in slug-type flows. Collier indicated that in long liquid slugs circulation zones were set up inside the slug that increased the heat transfer significantly. At the very low liquid velocities, the circulation, which is driven by buoyancy forces, has a very strong effect on heat transfer, since its magnitude is significant compared to the magnitude of the inertial forces. As the inertial forces grow, however, it becomes less important until at some liquid/gas velocity combination the inertial force balances the buoyancy force and negates its effect. Under microgravity conditions, this circulation will be very minimal, hence, the lower heat transfer coefficients for the μ-*g* data compared with the 1 *g* data at low liquid and gas flows.

In annular flows, the liquid film thickness is affected by gravity forces (particularly at lower gas velocities or low hold up) and, therefore, may influence the heat transfer. Clearly, the hydrodynamic influences of gravity, surface tension, and other pertinent forces will need to be pursued more fully in order to determine the exact cause of variations in the heat transfer coefficients reported under microgravity conditions.

Summary and Conclusions

Over the range of gas and liquid superficial velocities studied, the effect of gravity on the convective heat transfer coefficients in two-phase, two-component flows appears to be influenced by the magnitude of the liquid flow rate and the flow regime. Parametric studies involving changing gas velocities from 0.2 to 15 m/s at constant liquid velocities ranging from 0.24 to 3.0 m/s ($0.0001 < x < 0.1$) showed that for low liquid and gas velocities the 1 *g* data gave higher heat transfer rates than those taken at μ-*g* by 15%. When either the liquid or the gas velocities were increased, however, the difference in η between the two sets decreased until eventually the μ-*g* heat transfer coefficients were higher than the 1 *g* data. At the highest liquid velocities, the heat transfer coefficients in microgravity were up to 10% higher than their 1 *g* counterparts for all gas velocities. The uncertainty in the measurement of normalized heat transfer coefficient (normalized with single-phase data) was calculated to be on the order of 10% with a corresponding uncertainty in quality of 7.6%. Thus, the measured differences in the 1 *g* and μ-*g* heat transfer coefficients are significant at the low end of both liquid and gas velocities.

The effect of flow regime was found to be somewhat more complicated than was originally thought, changes in the heat transfer coefficients are not strictly related to changes in the flow regime. Major changes in flow regime between 1 *g* and μ-*g* data were not always evident when noticeable changes in the heat transfer coefficients were measured.

Acknowledgments

The authors would like to gratefully acknowledge the financial support provided by the User Development Program of the Canadian Space Agency, the Natural Science and Engineering Council of Canada (NSERC), and the University of Saskatchewan, Saskatoon, Saskatchewan, Canada.

References

[1]Merte, H., Jr., and Clark, J., "Boiling Heat Transfer with Cryogenic Fluids at Standard, Fractional, and Zero-Gravity," *Transactions of the American Society of Mechanical Engineers: Journal of Heat Transfer*, Vol. 88, No. 1, 1966, pp. 1–8.

[2]Siegel, R., "Effects of Reduced Gravity on Heat Transfer," *Advances in Heat Transfer*, edited by J. P. Hartnett and T. F. Irvine Jr., Vol. 4, Academic Press, New York, 1967, pp. 143–228.

[3]Papell, S. S., "An Instability Effect on Two-Phase Heat Transfer for Subcooled Water Flowing Under Conditions of Zero Gravity," American Rocket Society 17th Annual Meeting and Space Flight Exposition, Santa Monica, CA, Nov. 1962.

[4]Reddy Karri, S. B., and Mathur, V. K., "Two-Phase Flow Regime Map Predictions Under Microgravity," *AIChE Journal*, Vol. 34, No. 1, 1988, pp. 137–139.

[5]Zhao, L., and Rezkallah, K. S., "Gas-Liquid Flow Patterns at Microgravity Conditions," *International Journal of Multiphase Flow*, Vol. 19, No. 5, 1993, pp. 751–763.

[6]Dukler, A. E., Fabre, J. A., McQuillen, J. B., and Vernon, R., "Gas-Liquid Flow at Microgravity Conditions: Flow Patterns and Their Transitions," *International Journal of Multiphase Flow*, Vol. 14, No. 4, 1988, pp. 389–400.

[7]Feldmanis, C. J., "Pressure and Temperature Changes in Closed

Loop Forced Convection Boiling and Condensing Processes Under Zero Gravity Conditions," *Proceedings of the Institute of Environmental Sciences' 1966 Annual Technical Meeting*, Inst. of Environmental Science, Mt. Prospect, IL, 1966, pp. 455–461.

[8]Hill, W. S., and Best, F. R., "Definition of Two-Phase Flow Behaviors for Spacecraft Design," Air Force Phillips Lab., Final Rept. Contract F29601-88-C-0062, Kirtland AFB, NM, 1991.

[9]Rite, R. W., and Rezkallah, K. S., "An Investigation of Transient Effects on Heat Transfer Measurements in Two-Phase, Gas-Liquid Flows Under Microgravity Conditions," *ASME Heat Transfer in Microgravity Systems*, edited by S. S. Sadhal and A. Hashemi, Vol. 235, 1993, pp. 49–57.

[10]Coleman, H. W., and Steele, W. G., Jr., *Experimentation and Uncertainty Analysis for Engineers*, Wiley, New York, 1989, pp. 36–81.

[11]Chakroun, W., Taylor, R. P., Steele, W. G., and Coleman, H. W., "Bias Error Reduction in Experimental Results by Presentation as a Ratio to a Baseline Experiment—A Heat Transfer Case Study," AIAA Paper 93-0922, Jan. 1993.

[12]Zhao, L., and Rezkallah, K. S., "Pressure Drop in Two-Phase Annular Flow at Microgravity Conditions," AIAA Paper 93-0572, Jan. 1993.

[13]Vijay, M. M., Aggour, M. A., and Sims, G. E., "A Correlation of Mean Heat-Transfer Coefficients for Two-Phase Two-Component Flow in a Vertical Tube," *Proceedings of the 6th International Heat Transfer Conference*, Vol. 5, Hemisphere, Washington, DC, 1982, pp. 367–372.

[14]Collier, J. G., *Convective Boiling and Condensation*, 1st ed., McGraw-Hill, New York, 1972, pp. 392–395.